Collision Frequency of Artificial Satellites: The Creation of a Debris Belt

DONALD J. KESSLER AND BURTON G. COUR-PALAIS

NASA Johnson Space Center, Houston, Texas 77058

As the number of artificial satellites in earth orbit increases, the probability of collisions between satellites also increases. Satellite collisions would produce orbiting fragments, each of which would increase the probability of further collisions, leading to the growth of a belt of debris around the earth. This process parallels certain theories concerning the growth of the asteroid belt. The debris flux in such an earth-orbiting belt could exceed the natural meteoroid flux, affecting future spacecraft designs. A mathematical model was used to predict the rate at which such a belt might form. Under certain conditions the belt could begin to form within this century and could be a significant problem during the next century. The possibility that numerous unobserved fragments already exist from spacecraft explosions would decrease this time interval. However, early implementation of specialized launch constraints and operational procedures could significantly delay the formation of the belt.

INTRODUCTION

Since the beginning of the space age, thousands of satellites have been placed in earth orbit by various nations. These satellites may be grouped into three categories: payloads, rocket motors, and debris associated with the launch or breakup of a particular payload or rocket; most satellites fall into the last category. Because many of these satellites are in orbits which cross one another, there is a finite probability of collisions between them. Satellite collisions will produce a number of fragments, some of which may be capable of fragmenting another satellite upon collision, creating even more fragments. The result would be an exponential increase in the number of objects with time, creating a belt of debris around the earth.

This process of mutual collisions is thought to have been responsible for creating most of the asteroids from larger planetlike bodies. The time scale in which this process is taking place in the asteroid belt is of the order of billions of years. A much shorter time scale in earth orbit is suggested by the much smaller volume of space occupied by earth-orbiting satellites compared to the volume of space occupied by the asteroids.

Conceivably, a significant number of small satellite fragments already exist in earth orbit. Fragments which are undetected by radar are likely to have been produced from 'killer satellite' tests and the accidental explosions of rocket motors. Although some work has already been completed to estimate the number of these fragments, further investigations in this area are still required.

This paper will determine possible time scales for the growth of a 'debris belt' from collision fragments and will predict some of the possible consequences of continued unrestrained launch activities. This will be accomplished by applying techniques formerly developed for studying the evolution of the asteroid belt. A model describing the flux from the known earth-orbiting satellites will first be developed. The results from this model will then be extrapolated in time to predict the collision frequency between satellites. The hypervelocity impact phenomena will then be examined to predict the debris flux resulting from collisions. Other sources and sinks for debris will be discussed, and the effects of atmospheric drag will be predicted. These results will be applied to design requirements for three types of space missions in the future. The potential, or upper limit, debris flux will then be discussed. Although further studies are recommended, the conclusion is reached by this study that over the next few decades a significant amount of debris could be generated by collisions, affecting future spacecraft designs.

This paper is not subject to U.S. copyright. Published in 1978 by the American Geophysical Union.

Paper number 8A0210.

SATELLITE ENVIRONMENT MODEL

A model describing the environment resulting from orbiting satellites was constructed by first calculating the spatial density (average number of satellites per unit volume) as a function of distance from the earth and geocentric latitude. Flux (number of impacts per unit area per unit time) was then related to spatial density through the relative impact velocities. This technique was also used to model the collision frequency in the asteroid belt [*Kessler*, 1971].

Orbital perturbations can be expected to cause the orbital argument of perihelion and right ascension of ascending node to change fairly rapidly, causing these two distributions to be nearly random. This randomness was observed [*Brooks et al.*, 1975] and led to a uniform distribution in the spatial density as a function of geocentric longitude. The model was thus reduced to determining the spatial density S as a function of distance from the surface of the earth R and geocentric latitude β. To construct the model, volume elements were defined as $\Delta R = 50$ km and $\Delta\beta = 3°$. The spatial density in each of these volume elements was found by calculating the probability of finding each satellite in a particular volume element and then summing these probabilities. Spatial density is then this sum divided by the volume of the volume element.

The April 30, 1976, Satellite Situation Report [*NASA*, 1976] contains a total of 3866 satellites, indicating that as of this date a total of 3866 were being tracked, most by radar in low earth orbit. The Satellite Situation Report is compiled from data provided by the Space Defense Center (SDC) and represents the most complete data available. Even so, it was found to be significantly incomplete by a test performed in 1976 [*Hendren and Anderson*, 1976], especially at altitudes below 500 km. In addition, the drop in radar sensitivity for objects smaller than 10 cm [*Brooks et al.*, 1975] and for objects at higher altitudes produces another bias in these data. Such deficiencies caused the calculated spatial densities to be too low; the implications of this result will be discussed in later sections. Since only a statistical solution was required, sufficient accuracy was maintained by performing all calculations with a random sample consisting of 125 of the 3866 satellites.

The resulting spatial densities are given in Figures 1 and 2. Figure 1 shows the spatial density as a function of distance from the earth (averaged over latitude), while Figure 2 shows

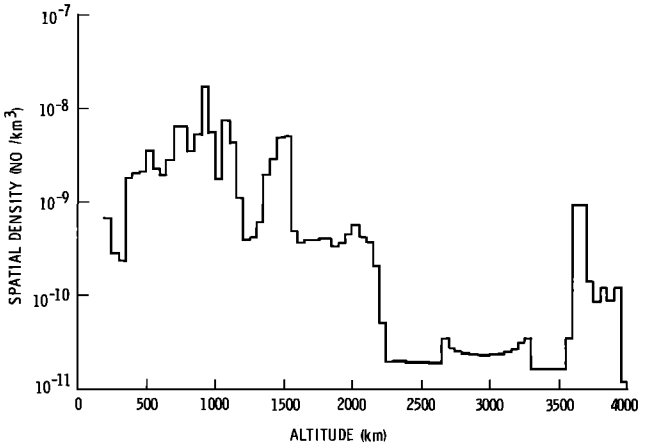

Fig. 1. Current distribution of satellites in earth orbit as observed by radar. A total of 3866 satellites are in the April 1976 catalog and are represented here.

the spatial density as a function of latitude for a few selected distances. Of particular note is that most of the satellites were found within about 2000 km of the earth, the peak density being found at about 900 km. Significant peaks were found at 1500 and 3700 km. In latitude, significant peaks were found between 30° and 35° and at >60°. For most latitudes the spatial density was found to be well within a factor of 2 of the average for that distance, although specific peaks were a factor of 3 or 4 from the average.

As a note of interest at this point, the impact rate on a particular spacecraft, dI/dt, can be quickly approximated from Figure 1 by using the equation

$$dI/dt = S\bar{V}_s A_c \tag{1}$$

where $\bar{V}_s$ is an average relative velocity, A_c is the cross-sectioned area of the spacecraft, and I is the total number of impacts with the spacecraft at time t. As will be shown later, $\bar{V}_s \simeq 7$ km/s. Therefore for a space station of 50-m radius, at 500-km altitude ($S \simeq 2.8 \times 10^{-9}$/km³ and $A_c = 7.9 \times 10^{-3}$ km²) the impact rate is 1.5×10^{-10}/s, or 4.9×10^{-3}/yr. This compares to about 3×10^{-3}/yr found by *McCarter* [1972] using a 1971 Satellite Situation Report containing 1805 objects. This impact rate is only slightly dependent on the space station orbital inclination: for inclinations less than 90° the rate varies by less than a factor of 2.

The collision rate between all satellites, dC/dt, is given by

$$dC/dt = \frac{1}{2}\int S^2 \bar{V}_s \bar{A}_{cc}\, dU \tag{2}$$

where C is the number of collisions between satellites, $\bar{A}_{cc}$ is an average collision cross-sectional area of the satellites, and dU is an element of volume. Thus both an average velocity and a collision cross-sectional area are required. These distributions and their resulting averages will be discussed now.

Velocity Distribution

The velocity distribution in each volume element was calculated by computing the relative velocity between each of the satellites in the random sample and then weighting the number having this velocity by the probability of finding the two satellites in the volume element. Two average velocities were found from these distributions: the average relative velocity $\bar{V}_s$ and the average collision velocity $\bar{V}_c$. To illustrate the difference between these averages, assume that there are three objects in a unit volume having velocities of 1, 2, and 3 km/s relative to one another. The average relative velocity would be 2 km/s. However, since the probability of collision is proportional to the relative velocity, for every collision at 1 km/s there will be two collisions at 2 km/s and three collisions at 3 km/s. The average collision velocity is thus 2.33 km/s. The average relative velocity can be shown to be the proper average to transform spatial density to flux and collision frequency, while the average collision velocity describes the average velocity at which objects would be observed to collide.

The results of these calculations for altitudes less than 2000 km were that $\bar{V}_s \simeq 7$ km/s and $\bar{V}_c \simeq 10$/km/s; these averages were found to be nearly independent of the volume element. At latitudes where the spatial density was large these average velocities were sometimes slightly smaller (by 1 or 2 km/s); however, this effect was small, so that $\bar{V}_s$ and $\bar{V}_c$ could be considered constant over all space below 2000 km.

Size Distribution

The size distribution of satellites was obtained from the radar cross section measurements. The data in Figure 3 were obtained during a 12-hour test of the perimeter acquisition radar (PAR) on July 31, 1976 [*Hendren and Anderson*, 1976]. The purpose of this test was to determine PAR's capability to detect and track objects that were not in the Space Defense Center catalog. The results of the test concluded that the SDC catalog was 18% deficient, and the implications of these results will be discussed later. However, the PAR data have other applications, since they represent a 'point-in-time' sampling of the satellite data and were gathered by a single instrument. Thus these data were used to analyze the satellite size distribution.

In an individual case the physical cross section A_c of an object may be orders of magnitude different from its radar cross section σ [*Ruck et al.*, 1970]. However, the difference may be small (less than a factor of 2) when an average physical cross section is compared to an average radar cross section

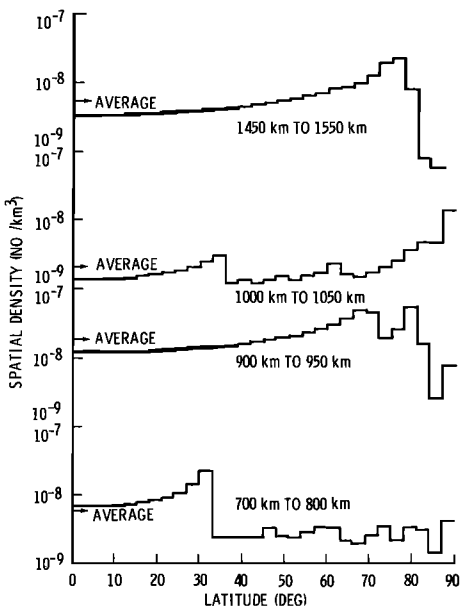

Fig. 2. Latitude variation in spatial density at selected altitudes. At most latitudes the spatial density is within a factor of 2 of the average at that distance.

21562202a, 1978, A6, Downloaded from https://agupubs.onlinelibrary.wiley.com/doi/10.1029/JA083iA06p02637 by Carnegie Mellon University, Wiley Online Library on [15/02/2026]. See the Terms and Conditions (https://onlinelibrary.wiley.com/terms-and-conditions) on Wiley Online Library for rules of use; OA articles are governed by the applicable Creative Commons License

resulting from the observation of many objects. But when the linear dimensions of an object become small compared to the wavelength, Rayleigh scattering causes the radar cross section to be much smaller than the physical cross section. This drop in radar sensitivity was at least partially responsible for the drop in number for sizes smaller than 0.03 m² shown in Figure 3. Hence the assumption was made that for $\sigma \geq 0.02$ m², $A_c = \sigma$. For $\sigma < 0.02$ m², $A_c \simeq k\sigma$, where k approaches 6 at the smaller values of σ in Figure 3. This correction for Rayleigh scattering produced only minor changes in the overall collision process.

Also plotted in Figure 3 is the distribution of total area of satellites. This distribution is of interest, since collision probabilities are related to area. The distribution suggests that most collisions will involve objects between the sizes of 1- to 100-m² cross section. The average cross section $\bar{A}_c = 1.5$ m² was found by dividing the integral of the area curve by the integral of the number curve.

However, the average collision cross section $\bar{A}_{cc}$ must include the finite size of both objects. Collision cross section is related to the physical cross section of two objects by

$$A_{cc} = (A_{ci}^{1/2} + A_{cj}^{1/2})^2 \quad (3)$$

where A_{ci} and A_{cj} are the physical cross sections of objects i and j, respectively. The collision cross section was calculated between each of the sizes in Figure 3, weighted according to the probability of those sizes colliding, and then averaged. The results were that $\bar{A}_{cc} \simeq 4$ m² and will be assumed to be independent of the volume element.

When the data in Figure 3 were compared with the SDC catalog data, the PAR radar cross sections were found to be about 50% less, on the average, than those of the SDC. This indicates an additional calibration uncertainty between the two radar systems. When combined with the uncertainty between radar and physical cross sections, the value of $\bar{A}_{cc}$ may range from about 2 m² to 12 m².

Thus (2) was integrated over the space between 150-km and 4000-km altitude by using $\bar{V}_s = 7$ km/s and $\bar{A}_{cc} = 4$ m² to give a collision rate of 0.013 collisions/yr, but this rate could range

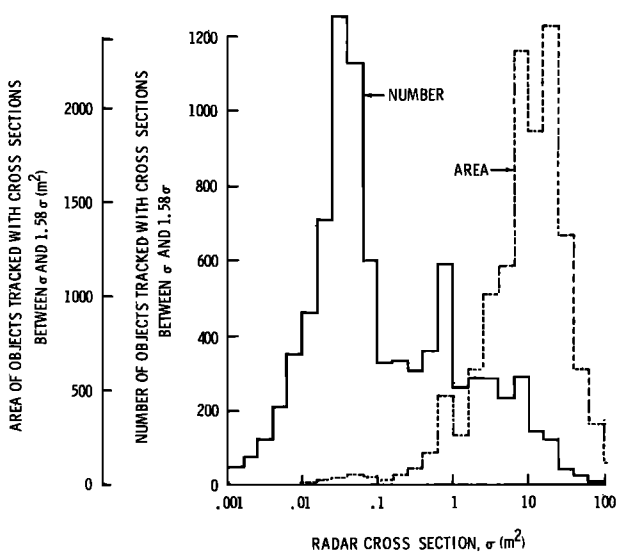

Fig. 3. Size distribution of earth-orbiting satellites observed by radar. The largest number of satellites have a radar cross section of about 0.04 m², while the largest area contribution is around a radar cross section of 10 m².

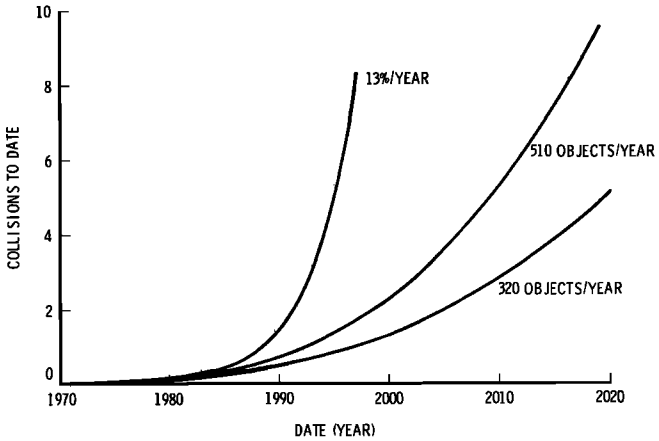

Fig. 4. Total collisions by the given date under various growth assumptions. The first collision is expected between 1989 and 1997.

from 0.007 to 0.039 collisions/yr, owing to the uncertainty in the relationship between the real and radar cross sections. These collision rates could be significantly higher if a large number of unobserved satellites exist.

Extrapolation Into the Future

Between 1968 and 1974 the net number of trackable objects in space increased at the rate of about 320 objects/yr [*Brooks et al.*, 1975]. From 1975 to the present that rate increased to 510/yr [*NASA*, 1974, 1975, 1976]. The period from 1966 to the present could be summarized by an increase of 13%/yr.

If it is assumed that the same pattern of debris buildup continues, then the number of collisions C by time t is found by integrating (2) over time, where the spatial density is then a function of time and proportional to the number of objects in space.

Figure 4 shows the results of such an integration, using the three different buildup rates. Note that under the more conservative assumption (320 objects/yr) the first collision would be expected around 1997. However, at a growth rate of 13%/yr this collision would occur around 1989. If the average collision cross section is overestimated by a factor of 2, the first collision could be as late as the year 2005, while an underestimation by a factor of 3 results in a first collision between 1985 and 1990 under any of the growth assumptions. The presence of unobserved satellites would move these dates even closer to the present. Thus unless significant changes are made in the method of placing objects into space, fragments from intercollisions will probably become a source of additional space debris by the year 2000, perhaps much earlier. The significance of this new source is seen by taking a closer look at the hypervelocity impact phenomenon.

Hypervelocity Impacts

The average impact velocity of 10 km/s ensures that almost all of the earth-orbiting objects will exhibit hypervelocity impact characteristics when they collide. Both objects will be subjected to very high instantaneous pressures ($\geq 10^{12}$ dyn/cm²), the strong shock waves causing melting and possible vaporization in the immediate region of the impact. A crater, or hole, will be formed, the molten ejected mass coalescing into more or less spherical particles. In addition, the shock waves, particle fragments hitting other surfaces, and vapor pressure may cause fragmentation outside the cratered region,

21562202a, 1978, A6, Downloaded from https://agupubs.onlinelibrary.wiley.com/doi/10.1029/JA083iA06p02637 by Carnegie Mellon University, Wiley Online Library on [15/02/2026]. See the Terms and Conditions (https://onlinelibrary.wiley.com/terms-and-conditions) on Wiley Online Library for rules of use; OA articles are governed by the applicable Creative Commons License

possibly resulting in the catastrophic disruption of both objects. This process has been studied for some time, mostly from the standpoint of protection of spacecraft from meteoroids, crater formation on the moon, and fragmentation of rocks on the lunar surface or in the asteroid belt. Because of the parallel between the potential formation of an earth-orbiting debris belt and the hypothetical formation of the asteroid belt, and because of the availability of data concerning impacts into solid, homogeneous objects, these data will be discussed first.

IMPACTS INTO SOLID STRUCTURES AND BASALT

Hypervelocity impacts into solid structures can be divided into two groups: catastrophic and noncatastrophic. A noncatastrophic collision results from the collision of two masses M_1 and M_2, where M_1 is much smaller than M_2 by an amount

$$M_2 > \Gamma' M_1 \tag{4}$$

where Γ' is a function of the impact velocity and the structure and materials of M_1 and M_2. In noncatastrophic collisions, only M_1 is destroyed, and a crater is produced in M_2, ejecting a total mass of M_e, which may be expressed as

$$M_e = \Gamma M_1 \tag{5}$$

where Γ is also a function of the impact velocity and the structure and materials of M_1 and M_2.

If M_1 is larger than the amount given in (4), then not only is a crater produced in M_2, but the entire structure of M_2 begins to fragment. This process is referred to as a catastrophic collision. These additional fragments are usually larger than the fragments from the crater and are ejected at a much slower velocity. The mass ejected from a catastrophic collision is

$$M_e = M_1 + M_2 \tag{6}$$

The ejected mass has also been shown to be proportional to the impact kinetic energy [*Moore et al.*, 1965; *Dohnanyi*, 1971]. Thus the values for Γ and Γ' will vary as V^2. At 10 km/s the values of Γ and Γ' for basalt are 500 and 25,000, respectively [*Dohnanyi*, 1971]. That is, for basalt, if M_2 is greater than 25,000 times M_1, then the ejected mass resulting from a collision between M_1 and M_2 at 10 km/s is 500 times M_1. If M_2 is less than 25,000 times M_1, then the collision is catastrophic. These results are summarized in Table 1, along with the results for glass and 1100-0 aluminum (low strength, high ductility). The glass and aluminum tests were performed by the Ames Research Center and the General Motors Defense Research Laboratories for the Johnson Space Center.

The number of small fragments of mass M and larger ejected from a noncatastrophic collision can be expressed as

$$N = K(M/M_e)^{\eta} \tag{7}$$

TABLE 1. Hypervelocity Impact Parameters

Material	Γ'	Γ
Basalt	25,000	500
Glass	120,000	2,000
1100-0 aluminum	2,600	130
Spacecraft structure	>115*	115

Γ' is the minimum ratio of target mass to projectile mass causing catastrophic disruption at 10 km/s. Γ is the ratio of ejected mass to projectile mass in a noncatastrophic collision at 10 km/s.

*No tests have been performed to obtain this value. This lower limit follows from the definitions of Γ' and Γ.

where K and η are constants. From tests performed on basalt, $K = 0.4$, and $\eta = -0.8$ [*Gault et al.*, 1963; *Dohnanyi*, 1971]. From these results and associated modeling [*Kessler*, 1971] it was concluded that the asteroid belt must include particles as small as dust grains. Of course, the objects in the asteroid belt are solid chunks of material, unlike the anthropogenic satellites in earth orbit.

IMPACTS INTO SPACECRAFT STRUCTURES

The objects expected to collide in earth orbit consist of predominantly scientific and military satellites, rocket motors, and fragments of the same caused by malfunctions or deliberate destruction. The proportion of solid chunks of material will be very small, and the majority of collisions will be between open and closed structures filled with equipment. Thus the typical object will be a nonhomogeneous mass with discontinuities and many voids. The only reported hypervelocity tests where fragment distributions were obtained for 'typical' space structures, with internal components, were performed by Langley Research Center [*Bess*, 1975]. The tests showed that for these particular configurations the same general ejected mass and fragment size distribution laws established for the solid objects also apply to spacecraft structures.

When these results were scaled to 10 km/s, a value of $\Gamma = 115$ was obtained for spacecraft structures. That is, in a noncatastrophic collision between a spacecraft structure and smaller object at 10 km/s the ejected mass would be 115 times the mass of the smaller object. Note from Table 1 that this value is not too different from that for solid 1100-0 aluminum. No tests have been performed to try to duplicate a catastrophic collision involving a spacecraft structure. Obviously, if the crater produced in a 'noncatastrophic' collision is larger than the satellite, then the collision is catastrophic; thus Γ' must be greater than 115 and by analogy to solid objects is likely to be much larger than 115.

When normalized by the total ejected mass, as in (7), the distribution of fragments from spacecraft structures looks very similar to that of basalt. Values of $K = 0.89$ and $\eta = -0.8$ were obtained from one test into the spacecraft structure, and $K = 0.69$ and $\eta = -0.84$ were obtained from the other test [*Bess*, 1975]. The velocities of fragments, measured from a 400-frame/s film, were found to be very slow, about 10–30 m/s. Most of the fragment mass from basalt targets is slower than 100 m/s [*Zook*, 1967].

Thus for collisions between earth-orbiting objects the following relationship was adopted:

$$M_e = 115 M_1 \tag{8}$$

when $M_2 > 115 M_1$. If $M_2 < 115 M_1$, then $M_e = M_2$ (the mass of M_1 was assumed to be small or lost). The number of fragments of mass M and larger resulting from the collision is given by

$$N = 0.8(M/M_e)^{-0.8} \tag{9}$$

SATELLITE MASS

Before these impact equations can be used, the individual mass of each satellite is required. Some of these masses are available, but not in one source. Mass and areas for a few payloads and rocket motors were found in several publications [*Bowman*, 1963; *Corliss*, 1967; *Martin*, 1967; *Von Braun and Ordway*, 1975; *Aerospace Defense Command*, 1977], and these data are plotted in Figure 5. Also plotted is the debris resulting from the breakup of a Centaur D-IT rocket [*Drago and Edge-*

21562202a, 1978, A6, Downloaded from https://agupubs.onlinelibrary.wiley.com/doi/10.1029/JA083iA06p02637 by Carnegie Mellon University, Wiley Online Library on [15/02/2026]. See the Terms and Conditions (https://onlinelibrary.wiley.com/terms-and-conditions) on Wiley Online Library for rules of use; OA articles are governed by the applicable Creative Commons License

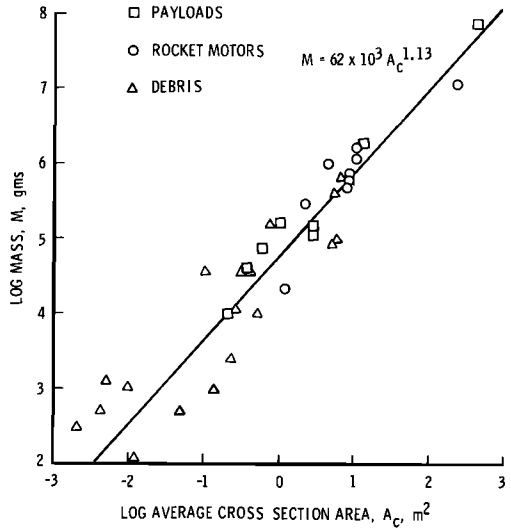

Fig. 5. Satellite mass versus average cross section.

combe, 1974]. The data were found to fit the relationship

$$M = 62 \times 10^3 A_c^{1.13} \quad (10)$$

where M is the mass of the satellite in grams and A_c is its average cross section in square meters. The slope of this fit was expected to be between 1.0 (which would be true of hollow structures with constant thickness walls) and 1.5 (which would be true of structures having a constant mass density). The value of 1.13 fell within this range.

Therefore masses were assigned to each of the sizes shown in Figure 3, according to (10). The amount of mass ejected in collisions between each size was calculated by using (8); however, the ejected mass was not allowed to exceed the mass of the larger object (the target mass). Each collision was then weighted according to its probability of occurrence in order to obtain an average mass ejected per collision. A result of 870 kg/collision was obtained. A detailed examination revealed that most mass resulted from satellites between 16 and 40 m² being impacted by satellites of 0.25 m² and larger; thus the ejected mass was limited in many cases by the mass available in the larger object.

This suggested that the average ejected mass may be fairly insensitive to (8). This sensitivity was tested by allowing the constant to vary by a factor of 10 on either side of 115, resulting in the average ejected mass varying from 440 to 1190 kg/collision. A more realistic lower limit for the constant in (8) is about a factor of 4 less (resulting in an average of 600 kg/collision), while the upper limit may be a factor of 10 or more larger, owing to the concept of catastrophic collisions (i.e., the value of Γ' in (4) could be 1150 or larger). Thus the measured size distribution of debris causes the average ejected mass to be fairly insensitive to the uncertainty in mass ejected during a collision. The sensitivity would increase if a sufficient number of objects smaller than 0.25 m² were known to be in earth orbit.

Thus on the basis of currently observed distribution of satellites an average of $M_e = 8.7 \times 10^5$ g is ejected in each collision shown in Figure 4.

Average Debris Flux Between 700 and 1200 km

By integrating (2) over the region of space between 700 and 1200 km a current collision rate of 0.01/yr was obtained, compared to 0.013/yr for all of space. Thus about 77% of the collisions were found to occur within this volume. The near-circular orbit of most objects found within this volume combined with the low ejection velocity of most fragments was justification for assuming that 77% of the collisional fragments would also be found within this volume.

Thus an average debris flux for this volume of space was found by

$$F = (N/U)\bar{V}_s \quad (11)$$

where N is the average number of objects of mass M and larger found within volume U and F is the flux of debris of mass M and larger. This flux was computed as a function of time by increasing the 3866 satellites (1976 number) at the 'nominal' rate of 510/yr. It was calculated that 51% of these satellites are normally found within the volume of space between 700 and 1200 km. The collision rate within this volume was assumed to be 77% of that shown in Figure 4. The number of fragments generated by each collision is given by (9) where $M_e = 8.70 \times 10^5$.

The projected debris flux is shown in Figure 6 for the years 1990, 2020, and 2100, compared with the natural meteoroid flux [*Cour-Palais,* 1969] and the current (1976) debris flux. The curve for the current debris flux is flat for debris masses less than 200 g only because these sizes cannot currently be observed. Even so, for meteoroid mass greater than 0.3 g the current debris flux between 700 and 1200 km already exceeds the natural meteoroid flux. As is illustrated in Figure 6, a significant number of debris fragments smaller than 200 g will be generated in the future, further exceeding the meteoroid flux.

To illustrate the effect on future space missions, consider three types of missions. The first is an unmanned satellite having an average cross section of 10 m² (i.e., about 3.6-m diameter) and a desired average lifetime of 10 years. The area-time product of such a satellite would be 10^2 m² yr, so that the design flux, to ensure an average 10-yr lifetime, would be 10^{-2}/m² yr. If meteoroids are the only hazard, then Figure 6 predicts that the satellite should be designed to survive a 2×10^{-4} g

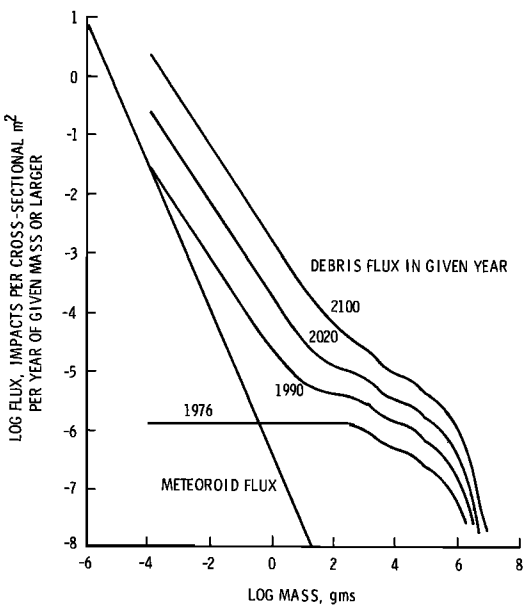

Fig. 6. Average debris flux between 700 and 1200 km; assumes that (1) the net satellite input rate is always 510/yr and (2) there is no atmospheric drag.

21562202a, 1978, A6, Downloaded from https://agupubs.onlinelibrary.wiley.com/doi/10.1029/JA083iA06p02637 by Carnegie Mellon University, Wiley Online Library on [15/02/2026]. See the Terms and Conditions (https://onlinelibrary.wiley.com/terms-and-conditions) on Wiley Online Library for rules of use; OA articles are governed by the applicable Creative Commons License

TABLE 2. Design Requirements for Three Hypothetical Missions

Mission Type	Unmanned	Skylab	Space Station
Design flux, impacts/m² yr	10^{-2}	10^{-4}	10^{-6}
Design meteoroid impact mass, g	2×10^{-4}	1×10^{-2}	4×10^{-1}
Year 2020, 1200-km altitude, debris design impact mass, g	1×10^{-2}	2.0	5×10^{5}
Altitude band where equilibrium debris flux exceeds meteoroid flux (assuming change to zero net satellite input after given year), km			
1980	none	750–1200	500–1200
2020	800–1200	550–1200	400–1500

meteoroid impact. The second type is a manned spacecraft having an average cross section of 100 m², a mission duration of 1 yr, and a desired probability of impact damage of less than 0.01. In this case the design flux would be 10^{-4}/m² yr, or about the same as the 1973–1974 Skylab mission. A meteoroid shield, weighing over 300 kg, was added to the Skylab structure in order to protect it against 10^{-2} g meteoroid impacts. The third type of mission is a large space station having an average cross section of 10,000 m² (i.e., a little over 100-m diameter), a mission duration of 10 yr, and a desired probability of impact damage of less than 0.1. The design flux would be 10^{-6}/m² yr, requiring protection against a 0.4-g meteoroid. These conditions are summarized in Table 2.

However, under certain conditions, as illustrated in Figure 6, the debris flux for these missions may exceed the meteoroid flux. By the year 2020 the unmanned, Skylab, and space station type missions may require protection against a 1×10^{-2} g, 2 g, and 5×10^{5} g debris particle, respectively. These missions would require more weight for impact protection. However, protection requirements against even a 100-g impact are so severe that a space station may have to either accept a much higher probability of impact damage or be restricted to altitudes where the debris flux is lower.

The increased risk of impact damage may lead to certain constraints being placed on launched satellites in order to reduce the projected debris hazard. For purposes of illustration it was assumed that beginning in 2020, the net satellite input rate of 510/yr is changed to zero. A zero rate can be maintained by ceasing all launch activity, returning a similar object for every object placed into orbit, or causing the reentry of unused objects. The results of this assumption are shown in Figure 7. Notice that the flux of fragments continues to increase after the year 2020.

OTHER SOURCES AND SINKS FOR DEBRIS

The effects of catastrophic collisions, collisions involving fragments from previous collisions, and the current number of unobserved small fragments all represent other sources of debris, increasing the results presented thus far. Each source has been looked at in some detail, and each is found to have a relatively small effect. (1) As was previously stated, the amount of mass produced per collision is mostly limited by the amount of mass available; thus the concept of catastrophic collisions could only about double the amount of fragment mass per collision. (2) With time, enough collisional fragments could be produced to become important in producing new collisional fragments. When these conditions apply, the number of objects will increase exponentially with time, even though no new objects may be placed into orbit by man. Some preliminary analysis indicated that the uncertainty in timing of this phenomenon is large but probably of the order of several hundred years. (3) The presence of objects that are too small to be detected by ground radar would imply that the current debris flux should be increased correspondingly. These objects must already exist as the results of numerous satellite explosions and other types of debris [*Neste et al.*, 1976]. However, a preliminary analysis concluded that the current number would have to be higher than the 1990 or 2020 projected number before the objects would become significant contributers to the collision-fragmentation process. Thus while the 18% deficiency observed in the SDC catalog [*Hendren and Anderson*, 1976] means that the current debris flux should be increased by 18%, the projected debris resulting from fragmentation would be increased by much less that 18%. In fact, if the unobserved population of small fragments requires that the total number of observed satellites be increased by a factor of 2.5, as suggested by *Brooks et al.* [1975], then the number of collisional fragments would be increased by less than 3%.

While these three additional sources may represent a small effect when they are taken individually, they may combine to produce a significant effect. For example, a 2.5 factor increase in the observed population, combined with a more realistic

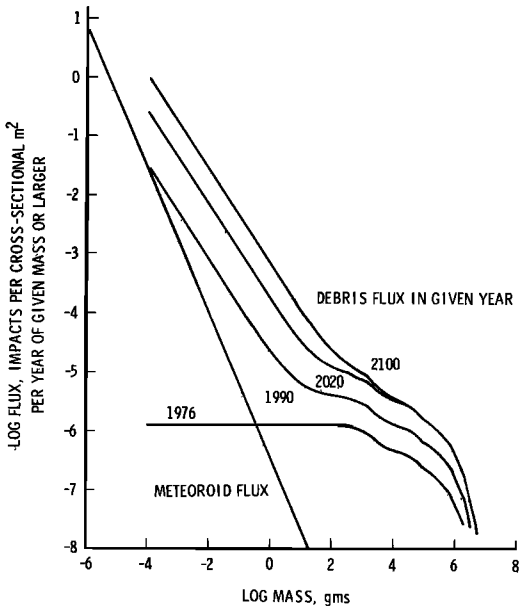

Fig. 7. Average debris flux between 700 and 1200 km; assumes that (1) the net satellite input rate changes from 510/yr to zero in the year 2020 and (2) there is no atmospheric drag.

21562202a, 1978, A6, Downloaded from https://agupubs.onlinelibrary.wiley.com/doi/10.1029/JA083iA06p02637 by Carnegie Mellon University, Wiley Online Library on [15/02/2026]. See the Terms and Conditions (https://onlinelibrary.wiley.com/terms-and-conditions) on Wiley Online Library for rules of use; OA articles are governed by the applicable Creative Commons License

value of catastrophic disruption mass ratio Γ', could double the number of collision fragments. Also, the exponential increase in fragments with time (source 2) could be observed much earlier than several hundred years, depending on the nature of catastrophic collisions, the projected number and size of future satellites, and the current number of unobserved small fragments. Meaningful analysis of this type must await more data.

Only a few 'sinks,' or removal mechanisms, exist for earth-orbiting satellites. They are basically only retrieval and atmospheric reentry. One could argue that as a result of catastrophic collisions, large objects disappear, and thus collision is a sink for these objects. However, hundreds of years are required before this becomes a significant sink, whereas collision is a much more important source of small fragments at a much earlier date. Thus for the near future it is accurate to think of collisions as only a source.

If retrieval is implemented, it could significantly alter the conclusions reached thus far. Collision rates are proportional to the collision cross section of satellites. Figure 3 reveals that 90% of the satellite area is contained in 20% of the satellites. Thus removal of large satellites could effectively slow down the collision rate. However, as the number of collision fragments increases, the concentration of area will move toward the more numerous, smaller objects, making it more difficult to slow down the fragmentation process by retrieval.

Atmospheric drag will eventually cause the reentry of many objects in orbit. Drag acts most quickly on small low-altitude objects and is a significant factor in reducing the number of satellites below 400 km, as is shown in Figure 1. The projected number of small fragments between 700 and 1200 km will be reduced from that shown in Figures 6 and 7 by the effects of atmospheric drag. However, since the collision frequency is low at altitudes less than 700 km, atmospheric drag will act as the primary source of fragments at these lower altitudes. That is, drag will act to remove collision fragments from the 700- to 1200-km region and drag them through these lower altitudes. Thus since atmospheric drag is the only natural sink for debris and since it may be an important source of debris at lower altitudes, it deserves a more detailed analysis.

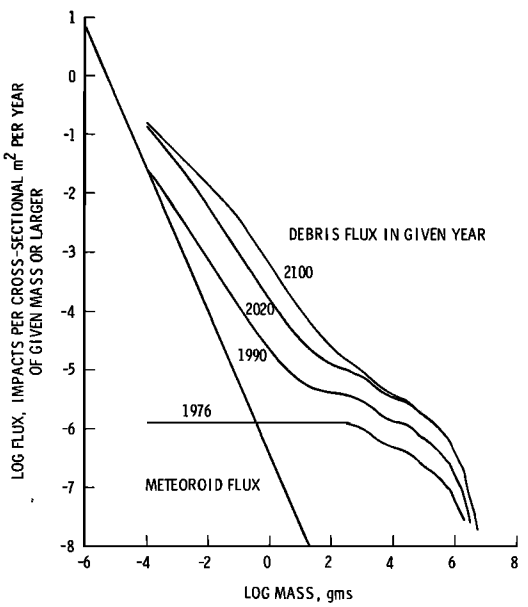

Fig. 8. Average debris flux at 1200 km; assumes that the net satellite input rate changes from 510/yr to zero in the year 2020.

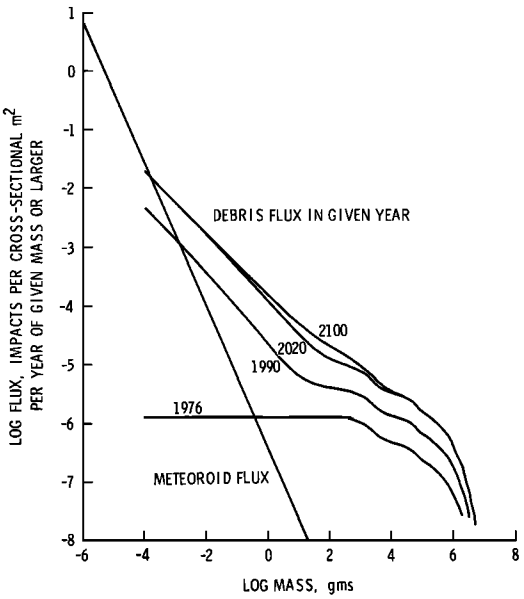

Fig. 9. Average debris flux at 800 km; assumes that the net satellite input rate changes from 510/yr to zero in the year 2020.

ATMOSPHERIC DRAG

Atmospheric drag will act to first circularize an orbit, then cause the object to spiral into the atmosphere. The speed at which this process works is proportional to the area to mass ratio of the object, as well as the atmospheric density at a given altitude [*Martin*, 1967]. With the use of the atmospheric model of *Lou* [1973], energy loss rates were calculated to obtain orbital decay times. The time for a 1-cm-radius sphere of mass density 2 g/cm³ (mass of 8.4 g) to change its altitude by 100 km for circular orbits of 800 km and 1200 km was calculated to be 32 yr and 455 yr, respectively. This compares to 110 yr and 2000 yr, respectively, calculated by *Martin* [1967] and 20 yr and 100 yr, respectively, calculated by *Brooks et al.* [1975]. The large range in values results from uncertainties in the atmospheric model and drag coefficients.

Lifetimes at a particular altitude were assumed to be the same as the calculated values for a circular orbit to decrease by 100 km. Of course, actual lifetimes could be longer or shorter, depending on orbital perigee or apogee. However, since most of the satellites within the 700- to 800-km band are in nearly circular orbits, this approximation should be fairly accurate. Lifetime as a function of particle size varies as particle radius, assuming a constant mass density.

Thus a model was developed which calculated the number of collisional fragments of a particular size which are produced during the lifetime of that size. Figure 8 gives the results of that model at 1200-km altitude. By comparison to Figure 7, drag had no effect on the debris design impact masses given in Table 1 for the year 2020. The change to a zero net satellite input rate in 2020 still led to an increased debris flux in 2100, although the flux of debris particles of less than 0.1 g was reduced by atmospheric drag.

Figure 9 gives the results of atmospheric drag at 800 km. In comparison with Figure 7 the debris design impact mass for an unmanned mission in the year 2020 was reduced, although it was still higher than the meteoroid design impact mass. For Skylab and space station type missions the debris flux was essentially unchanged by atmospheric drag. Of particular in-

21562202a, 1978, A6, Downloaded from https://agupubs.onlinelibrary.wiley.com/doi/10.1029/JA083iA06p02637 by Carnegie Mellon University, Wiley Online Library on [15/02/2026]. See the Terms and Conditions (https://onlinelibrary.wiley.com/terms-and-conditions) on Wiley Online Library for rules of use; OA articles are governed by the applicable Creative Commons License

terest in Figure 9 is that a change in the net satellite input rate to zero in the year 2020 resulted in a near-equilibrium being established for times after that date. That is, collisional fragments are being generated at the same rate as they are being removed by atmospheric drag. This equilibrium was reached almost immediately after the year 2020 for sizes smaller than about 0.1 g, while the sizes between 0.1 and 10^4 g were near equilibrium in 2020, reaching it by the year 2100. By comparing Figures 8 and 9 an equilibrium at 1200 km was reached for sizes smaller than 0.1 g by the year 2100 but at a flux level about a factor of 10 larger than that at 800 km.

These equilibrium debris levels suggest another way of looking at the future debris fluxes: that is, given a date to change from a net satellite input rate of 510/yr to zero, what will the equilibrium debris flux eventually become? For altitudes below 800 km the equilibrium will be reached almost immediately after the change to zero input date, whereas for altitudes up to 1200 km, several hundred years may be required, especially for the larger debris sizes. Figure 10 shows the average equilibrium debris flux at 800 km for various change input rate dates. Notice that even an early (1980) change to zero net input rate would eventually affect Skylab type missions at 800 km, whereas unmanned missions would not be affected at this altitude until a change after 2020. A similar curve for 1200-km altitude would be about a factor of 10 higher. The time required for atmospheric drag to drag a fragment through a particular altitude is inversely proportional to the atmospheric density at that altitude. Thus the average equilibrium debris flux at altitudes below 800 km (and actually above 800 km, up to 1200 km), was found by taking the ratio of the atmospheric density at that altitude to the atmospheric density at 800 km. Figure 11 gives that ratio of equilibrium fluxes. Thus for example, the equilibrium flux at 500 km was found by reducing the debris fluxes in Figure 10 by a factor of 30.

From this type of analysis the region of space where the debris flux could exceed the natural meteoroid flux was determined for the three types of missions. Table 2 summarizes these altitude bands, assuming a change to the zero net input rate in 1980 or 2020. An early (1980) change would prevent

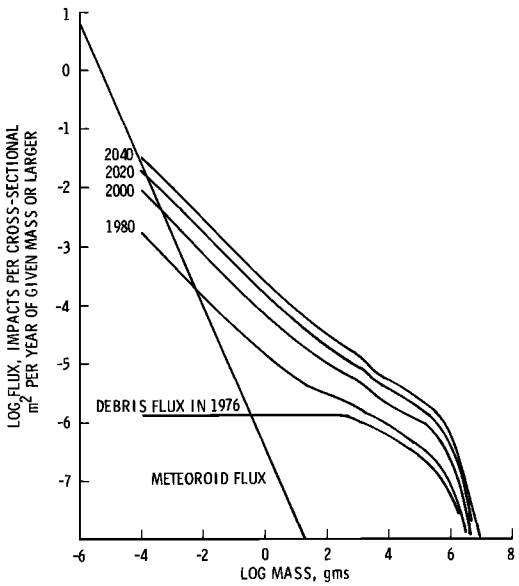

Fig. 10. Average equilibrium debris flux at 800 km; assumes that the net satellite input rate changes from 510/yr to zero in given year.

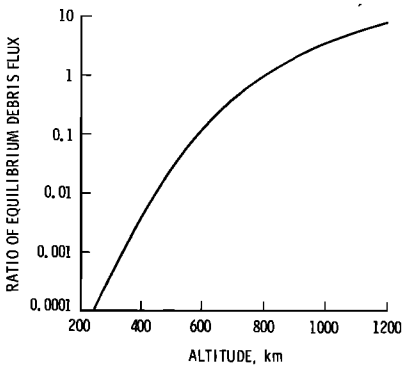

Fig. 11. Ratio of equilibrium debris flux at given altitude to flux at 800 km.

unmanned satellites from being affected by the debris flux anywhere in space. Skylab and space station type missions would be affected between 750 and 1200 km and 500 and 1200 km, respectively. However, if the change does not occur until the year 2020, the region of space where unmanned missions would be affected becomes 800–1200 km, and the Skylab and space stations regions affected expand to 550–1200 km and 400–1500 km, respectively. Thus an increase in the change date leads to larger regions of space where the debris flux could eventually exceed the meteoroid flux. The only obvious method of lowering this eventual equilibrium flux is to minimize the number of large satellites, either by a change in launch practices or by retrieval.

THE 'POTENTIAL' DEBRIS ENVIRONMENT

Thus far, the physical processes of collision and atmospheric drag have been applied to the observed distribution of satellites in earth orbit in an attempt to predict the time history of debris in earth orbit. However, it is known that satellites can fragment from other sources and that attempted modeling of incomplete data may predict the future debris flux inadequately.

Another approach might be to define the 'potential' debris flux and then develop arguments which would prevent this potential from being realized. This type of analysis would produce flux curves much higher than the previous curves, but the analysis would predict accurately what is possible, although not necessarily what is probable. A beginning point would be to assume that all satellites, through some unknown mechanism, become fragmented into some preferred but yet to be determined fragment size. The potential flux as a function of mass is then found by assuming that all of these fragments are of the preferred size. This potential flux is actually an envelope of single-size fluxes. As data become available that indicate that only some fraction of the total mass goes into a particular size interval, then the potential flux could be lowered appropriately in that size interval.

The average satellite mass was found (by using Figure 3 and (10)) to be 1.3×10^5 g, or a total 1976 satellite mass of 5×10^8 g. If this total mass were to fragment into debris of mass M, then the number of fragments would be

$$N = 5 \times 10^8 M^{-1} \quad (12)$$

If these fragments maintained the same orbits as the original 3866 satellites, then by using the same techniques as the original model, the 'average potential flux' between 700 and 1200 km was found and is shown in Figure 12. Note that if this

21562202a, 1978, A6, Downloaded from https://agupubs.onlinelibrary.wiley.com/doi/10.1029/JA083iA06p02637 by Carnegie Mellon University, Wiley Online Library on [15/02/2026]. See the Terms and Conditions (https://onlinelibrary.wiley.com/terms-and-conditions) on Wiley Online Library for rules of use; OA articles are governed by the applicable Creative Commons License

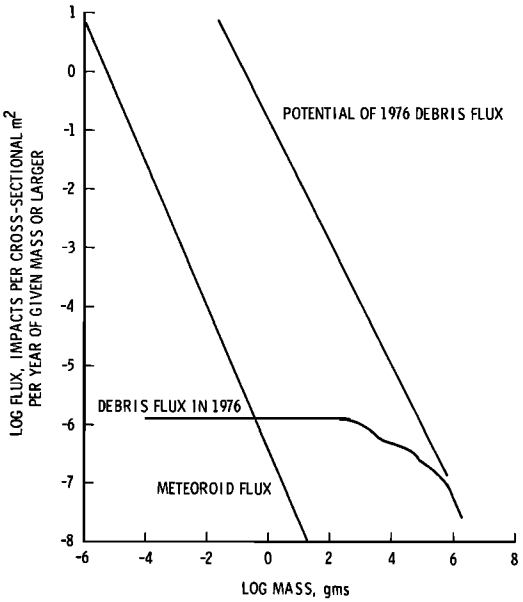

Fig. 12. Potential debris flux between 700 and 1200 km. Potential flux assumes that all satellites are fragmented into given mass.

potential were ever realized, all types of missions into this region would experience a flux level far in excess of the natural meteoroid flux. In fact, since it becomes impractical to protect against impacts larger than about 100 g, all missions would have to expect damage in certain regions of space.

The potential flux for other distances may be scaled from Figure 1. For example, the spatial density at 300 km was found from Figure 1 to be about a factor of 30 lower than the average between 700 and 1200 km; thus the debris curves in Figure 12 could be lower by this amount to obtain the 300-km fluxes.

As more mass is added to the system with time, the potential flux will increase correspondingly. The potential flux can be decreased as data become available. For example, at least 31 larger satellites, or about 1% of the total number of satellites, have already exploded in orbit [*Neste et al.*, 1976]. If fragmentation could be limited to these 31 explosions, then the potential flux could be reduced by a factor of 100. In addition, if it were found that only a small fraction of the fragmented mass were of a particular size or larger, then the potential flux for that size could be reduced further.

However, if fragmentation is maintained at 1%, or about 5 explosions per year, the potential flux would continue to increase until an equilibrium is reached with atmospheric drag. At 800 km this equilibrium would be about 4% of the potential flux shown in Figure 12 for fragments of 8.4 g and 0.4% for fragments of 8.4×10^{-3} g. Thus without meaningful data on the actual size distribution of fragments, the expected fragmentation rate, and the lifetime of these fragments it is difficult to lower the potential debris flux significantly.

Future Analysis Required

In order to reduce the uncertainty in the projected debris environment, additional data will be required on the effects of hypervelocity collisions between spacecraft, as well as the effects of other spacecraft fragmentation processes. Additional data on the number of small objects in space can be obtained by a detailed examination of individual launch and orbit injection procedures. The results of these studies should be tested by experiments designed to detect objects in orbit smaller than 10 cm. An optical experiment is described by *Neste et al.* [1976] which would detect debris in the 1-mm to 10-cm range. With the availability of improved input data, a model could be developed to include the results from explosions, the effects of collisions resulting from collision fragments, the effects of catastrophic collisions, and orbital changes resulting from collisions.

Various methods to stop or slow the formation of a debris belt should be studied. The model suggests that the most effective way would be to keep the number of large objects as small as practical. This could be accomplished by planning launches so that large objects can be caused to reenter when their usefulness is complete or by using the space shuttle concept to retrieve objects in orbit which no longer serve a useful function. Since it is impractical to retrieve the much larger number of large and small fragments, every effort should be made to prevent their production in space, either by explosion or by collision.

The evolution of the debris belt should be followed to its conclusion. As was pointed out by *Alfvén and Arrhenius* [1976], the consequence of many collisions is to change the orbits of objects to be more alike. This process may be responsible for creating 'jet streams' in the asteroid belt. With time, according to Alfvén, these jet stream orbits will become identical, and a single planet will accrete (billions of years in the future) at 2.8 AU. However, in the case of the earth the debris belt will be within the Roche's limit (less than 9000-km altitude), preventing accretion into a single object. Thus the end result, assuming that drag does not act fast enough, could be a ring system, similar to that around Saturn and Uranus.

Conclusions

A model has been developed which considers the major source and sink terms for the growth of the satellite population in earth orbit. While significant uncertainties exist, the following conclusions, if current trends continue, seem unavoidable:

1. Collisional breakup of satellites will become a new source for additional satellite debris in the near future, possibly well before the year 2000.
2. Once collisional breakup begins, the debris flux in certain regions near earth may quickly exceed the natural meteoroid flux.
3. Over a longer time period the debris flux will increase exponentially with time, even though a zero net input rate may be maintained.
4. The processes which will produce these fragments are totally analogous to the processes that probably occurred in the formation of the asteroid belt but require a much shorter time.

Effective methods exist to alter the current trend without significantly altering the number of operational satellites in orbit. These methods include reducing the projected number of large, nonoperational satellites and improved engineering designs which reduce the frequency of satellite breakups from structural failure and explosions in space. Delay in implementation of these methods reduces their effectiveness.

Acknowledgments. We thank Joe M. Alvarez (NASA) for helpful discussions of past work in these areas, leading to further helpful discussion with Preston M. Landry (NORAD) and Larry Rice (SAI). We acknowledge suggestions by Herbert A. Zook and Andrew E. Potter (NASA) which led to changes in the content of this paper.

The Editor thanks D. R. Brooks and V. J. Drago for their assistance in evaluating this paper.

21562202a, 1978, A6, Downloaded from https://agupubs.onlinelibrary.wiley.com/doi/10.1029/JA083iA06p02637 by Carnegie Mellon University, Wiley Online Library on [15/02/2026]. See the Terms and Conditions (https://onlinelibrary.wiley.com/terms-and-conditions) on Wiley Online Library for rules of use; OA articles are governed by the applicable Creative Commons License

REFERENCES

Aerospace Defense Command, Average radar cross section (sq. m.) as of 1 July 1977, report, Peterson Air Force Base, Colo., 1977.

Alfvén, H., and G. Arrhenius, Evolution of the solar system, *NASA Spec. Publ. SP-345,* 1976.

Bess, T. D., Mass distribution of orbiting man-made space debris, *NASA Tech. Note TND-8108,* 1975.

Bowman, N. J., *The Handbook of Rockets and Guided Missiles,* Perastadion Press, Newtown Square, Pa., 1963.

Brooks, D. R., G. G. Gibson, and T. D. Bess, Predicting the probability that earth-orbiting spacecraft will collide with man-made objects in space, in *Space Rescue and Safety,* pp. 79–139, American Astronautical Society Publications Office, Tarzana, Calif., 1975.

Corliss, W. R., Scientific satellites, *NASA Spec. Publ. SP-133,* 1967.

Cour-Palais, B. G., Meteoroid environment model—1969 (near earth to lunar surface), *NASA Spec. Publ. SP-8013,* 1969.

Dohnanyi, J. S., Fragmentation and distribution of asteroids, Physical Studies of Minor Planets, *NASA Spec. Publ. SP-267,* 263–295, 1971.

Drago, V. J., and D. S. Edgecombe, A review of NASA orbital decay reentry debris hazard, *Rep. BMI-NVLP-TM-74-1,* Battelle Mem. Inst., Columbus, Ohio, 1974.

Gault, D. E., E. M. Shoemaker, and H. J. Moore, Spray ejected from the lunar surface by meteoroid impact, *NASA Tech. Note TND-1767,* 1963.

Hendren, J. K., and A. Anderson, Comparison of the perimeter acquisition radar (PAR) satellite track capability to the Space Defense Center (SDC) satellite catalogue—Unknown satellite track experiment, *Rep. SAI-77-701-HU,* Sci. Appl., Inc., Huntsville, Ala., 1976.

Kessler, D. J., Estimate of particle densities and collision danger for spacecraft moving through the asteroid belt, Physical Studies of Minor Planets, *NASA Spec. Publ. SP-267,* 595–605, 1971.

Lou, G. Y., Models of earth's atmosphere (90 to 2500 km), *NASA Spec. Publ. SP-8021,* 1973.

Martin, C. N., *Satellites Into Orbit,* translated from French by T. Schoeters, George G. Harrap Co. Ltd., London, 1967.

McCarter, J. W., Probability of satellite collision, *NASA Tech. Memo TMX-64671,* 1972.

Moore, H. J., D. E. Gault, and E. D. Heitowit, Change of effective target strength with increasing size of hypervelocity impact craters, Proceedings of 7th Hypervelocity Impact Symposium, vol. IV, Theory, p. 35, U.S. Army, Navy, Air Force, 1965. (Available from National Technical Information Service, Springfield, Va.)

NASA, Satellite Situation Report, vol. 14, Off. of Publ. Aff., Goddard Space Flight Center, Greenbelt, Md., 1974.

NASA, Satellite Situation Report, vol. 15, Off. of Publ. Aff., Goddard Space Flight Center, Greenbelt, Md., 1975.

NASA, Satellite Situation Report, vol. 16, Off. of Publ. Aff., Goddard Space Flight Center, Greenbelt, Md., 1976.

Neste, S. L., R. K. Soberman, K. Lichtenfield, and L. R. Eaton, The Sisyphus system—Evaluation, suggested improvements, and application to measurements of space debris, final report, contract NAS1-13407, Gen. Elec. Co., Philadelphia, Pa., 1976.

Ruck, G. T., D. E. Barrick, W. D. Stuart, and C. K. Krichbaum, *Radar Cross Section Handbook,* Plenum, New York, 1970.

Von Braun, W., and F. I. Ordway III, *History of Rockets and Space Travel,* Thomas Y. Crowell Company, New York, 1975.

Zook, H. A., The problem of secondary ejecta near the lunar surface, in *Saturn V/Apollo and Beyond,* pp. EN-8-1 to EN-8-24, American Astronautical Society Publications Office, Tarzana, Calif., 1967.

(Received November 7, 1977;
revised February 10, 1978;
accepted February 22, 1978.)

21562202a, 1978, A6, Downloaded from https://agupubs.onlinelibrary.wiley.com/doi/10.1029/JA083iA06p02637 by Carnegie Mellon University, Wiley Online Library on [15/02/2026]. See the Terms and Conditions (https://onlinelibrary.wiley.com/terms-and-conditions) on Wiley Online Library for rules of use; OA articles are governed by the applicable Creative Commons License